# Scheme for Achieving a Topological Photonic Crystal by Using Dielectric Material

Long-Hua Wu and Xiao Hu*
*International Center for Materials Nanoarchitectonics (WPI-MANA), National Institute for Materials Science, Tsukuba 305-0044, Japan*
*Graduate School of Pure and Applied Sciences, University of Tsukuba, Tsukuba 305-8571, Japan*
(Received 10 February 2015; published 3 June 2015)

We derive in the present work topological photonic states purely based on conventional dielectric material by deforming a honeycomb lattice of cylinders into a triangular lattice of cylinder hexagons. The photonic topology is associated with a pseudo-time-reversal (TR) symmetry constituted by the TR symmetry supported in general by Maxwell equations and the $C_6$ crystal symmetry upon design, which renders the Kramers doubling in the present photonic system. It is shown explicitly for the transverse magnetic mode that the role of pseudospin is played by the angular momentum of the wave function of the out-of-plane electric field. We solve Maxwell equations and demonstrate the new photonic topology by revealing pseudospin-resolved Berry curvatures of photonic bands and helical edge states characterized by Poynting vectors.

DOI: 10.1103/PhysRevLett.114.223901 PACS numbers: 42.70.Qs, 03.65.Vf, 73.43.-f

*Introduction.*—The discovery of the quantum Hall effect (QHE) opened a new chapter of condensed matter physics with topology as the central concept [1–11]. Topological states are not only interesting from an academic point of view, but also expected to yield significant impacts to applications because robust surface (or edge) states protected by bulk topology provide possibilities for spintronics and quantum computation [12–17]. However, electronic systems with nontrivial topology confirmed so far are still limited in number, and most of them exhibit topological properties only at very low temperatures, which hinders their better understanding and manipulation indispensable for practical applications.

Photonic crystals are analogues of conventional crystals with the atomic lattice replaced by a medium of periodic electric permittivity and/or magnetic permeability [18]. Metamaterials are designed to generate electromagnetic (EM) properties such as negative index, magnetic lens, and so on, which are not available in nature [19]. Recently, it has been recognized that topological states characterized by unique edge propagations of an EM wave can be realized in photonic crystals based on gyromagnetic materials under external magnetic field, bi-anisoctroic metamaterials with coupled electric and magnetic fields where bi-anisotropy acts as effective spin-orbit coupling, and coupled resonator optical waveguides (CROWs) [20–31] (for a review see Ref. [32]).

In the present work, we propose a two-dimensional (2D) photonic crystal purely made of conventional dielectric material. We notice that a honeycomb lattice is equivalent to a triangular lattice of hexagonal clusters composed by six neighboring sites, and that, taking this larger hexagonal unit cell instead of the primitive rhombic unit cell of two sites (see Fig. 1), the Dirac cones at $K$ and $K'$ points in the first Brillouin zone of honeycomb lattice are folded to doubly degenerate Dirac cones at the $\Gamma$ point. It is then intriguing to observe that at the $\Gamma$ point there are two 2D irreducible representations in the $C_6$ symmetry group associated with odd and even parities respective to spatial inversion operation. Based on these properties, we propose opening a topologically nontrivial band gap by deforming the honeycomb lattice in a way that keeps the hexagonal clusters and preserves the $C_6$ symmetry (see Fig. 1). Solving Maxwell equations, we reveal explicitly that harmonic transverse magnetic (TM) modes hosted by the hexagonal cluster, working as "artificial atom" in the present scheme, exhibit electronic orbital-like $p$- and $d$-wave shapes and form photonic bands. We clarify that there is a pseudo-time-reversal (TR) symmetry constituted by the TR symmetry respected by Maxwell equations and the $C_6$ crystal

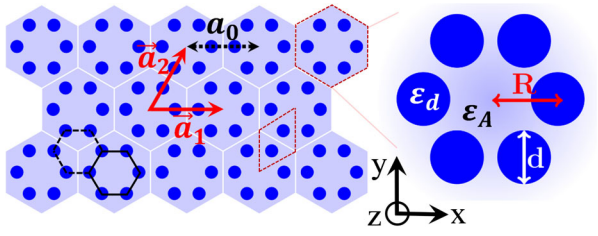


FIG. 1 (color online). Schematic plot of a triangular photonic crystal of "artificial atoms" composed by six cylinders of dielectric material. Dark gray (Red) dashed rhombus and hexagon are primitive cells of honeycomb and triangular lattices. The solid black hexagon labels an artificial atom, while the dashed black one marks the interstitial region among artificial atoms. $\vec{a}_1$ and $\vec{a}_2$ are unit vectors with length $a_0$ as the lattice constant. Right panel: enlarged view of a hexagonal cluster with $R$ the length of the hexagon edge and $d$ the diameter of cylinders. $\varepsilon_d$ and $\varepsilon_A$ are dielectric constants of cylinders and surrounding environment.

 

symmetry upon design, which behaves in the same way as TR symmetry in electronic systems and renders the Kramers doubling in the present photonic system. This intimately gives the correspondence between the positive and negative angular momenta of the wave function of the out-of-plane electric field and the up and down spins of the electron. Evaluating the Berry curvatures of bulk photonic bands and the edge states for finite systems, we demonstrate the emergence of the topological phase. With the simple design free of requirements on any external field and gyromagnetic or bi-anisotropic materials, the present topological photonic state purely based on dielectric material is expected to be promising for future applications.

*Artificial atom and pseudospin.*—Let us consider harmonic TM modes of the EM wave, namely, those of finite out-of-plane $E_z$ and in-plane $H_x$ and $H_y$ components with others being zero, in a dielectric medium (for coordinates see Fig. 1). For simplicity, the real electric permittivities of both cylinders ($\varepsilon_d$) and environment ($\varepsilon_A$) are taken frequency independent in the regime under consideration. The master equation for a harmonic mode of frequency $\omega$ is then derived from the Maxwell equations [33]

$$\left[\frac{1}{\varepsilon(\mathbf{r})}\nabla\times\nabla\times\right]E_z(\mathbf{r})\hat{z}=\frac{\omega^2}{c^2}E_z(\mathbf{r})\hat{z}, \tag{1}$$

with $\varepsilon(\mathbf{r})$ the position-dependent permittivity and $c$ the speed of light. The magnetic field is given by the Faraday relation $\mathbf{H}=-[i/(\mu_0\omega)]\nabla\times\mathbf{E}$, where the magnetic permeability $\mu_0$ is presumed as that of vacuum. The Bloch theorem applies for the present system when $\varepsilon(\mathbf{r})$ is periodic as shown in Fig. 1. Note, however, that the master equation (1) describes the EM waves instead of electrons carrying on the spin degrees of freedom, with the most prominent difference lying at the response upon TR operation. Equation (1) is solved in momentum space using package MIT PHOTONIC BANDS (MPB) [34]. For simplicity, we consider first a system infinite in the $z$ direction which reduces the problem to two dimensions.

We start from a honeycomb lattice of dielectric cylinders, and deform it in such a way as to keep the hexagonal clusters composed by six neighboring cylinders and the $C_6$ symmetry. Now the alignment of dielectric cylinders is more convenient to be considered as a triangular lattice of hexagonal artificial atoms. There are two 2D irreducible representations in the $C_6$ symmetry group associated with the triangular lattice: $E'$ and $E''$ with basis functions $x(y)$ and $xy(x^2-y^2)$, corresponding to odd and even spatial parities, respectively [35]. As can be seen in Fig. 2(a) for the $E_z$ field at the $\Gamma$ point, artificial atoms carry $p_x(p_y)$ and $d_{xy}(d_{x^2-y^2})$ orbitals, with the same symmetry as those of electronic orbitals of conventional atoms in solids.

We now examine matrix representations of $\pi/3$ rotation and its combinations for the orbitals $p_x(p_y)$ and $d_{xy}(d_{x^2-y^2})$. Since $p_x(p_y)$ behave in the same way as $x(y)$, it is easy to see

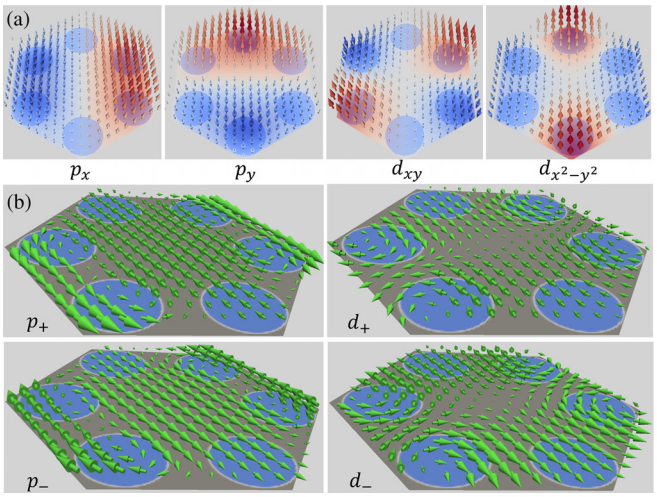


FIG. 2 (color online). (a) Electric fields $E_z$ of the $p_x(p_y)$ and $d_{xy}(d_{x^2-y^2})$ photonic orbitals hosted by the artificial atom at the $\Gamma$ point. (b) Magnetic fields associated with $E_z$ fields with wave functions of positive and negative angular momenta $p_\pm=(p_x\pm ip_y)/\sqrt{2}$ and $d_\pm=(d_{x^2-y^2}\pm id_{xy})/\sqrt{2}$. The angular momentum of the wave function of the $E_z$ field constitutes the pseudospin in the present photonic crystal.

$$D_{E'}(C_6)\begin{pmatrix}p_x\\p_y\end{pmatrix}=\begin{pmatrix}\frac{1}{2}&-\frac{\sqrt{3}}{2}\\\frac{\sqrt{3}}{2}&\frac{1}{2}\end{pmatrix}\begin{pmatrix}p_x\\p_y\end{pmatrix}. \tag{2}$$

It is noticed that $\mathcal{U}=[D_{E'}(C_6)+D_{E'}(C_6^2)]/\sqrt{3}=-i\sigma_y$ with $D_{E'}(C_6^2)\equiv D_{E'}^2(C_6)$ is associated with the $\pi/2$ rotation of $p_x(p_y)$ ($\sigma_y$ being the Pauli matrix). Therefore, $\mathcal{U}^2(p_x,p_y)^{\mathrm{T}}=-(p_x,p_y)^{\mathrm{T}}$, which is consistent with the odd parity of $p_x(p_y)$ with respect to spatial inversion. Similarly, one has

$$D_{E''}(C_6)\begin{pmatrix}d_{x^2-y^2}\\d_{xy}\end{pmatrix}=\begin{pmatrix}-\frac{1}{2}&-\frac{\sqrt{3}}{2}\\\frac{\sqrt{3}}{2}&-\frac{1}{2}\end{pmatrix}\begin{pmatrix}d_{x^2-y^2}\\d_{xy}\end{pmatrix}, \tag{3}$$

which is same as $D_{E'}(C_6^2)$ because the basis functions are now bilinear of $x(y)$. It is then straightforward to check that $[D_{E''}(C_6)-D_{E''}(C_6^2)]/\sqrt{3}=\mathcal{U}$ is associated with a $\pi/4$ rotation of $d_{xy}(d_{x^2-y^2})$, which yields $\mathcal{U}^2(d_{x^2-y^2},d_{xy})^{\mathrm{T}}=-(d_{x^2-y^2},d_{xy})^{\mathrm{T}}$.

We compose the antiunitary operator $\mathcal{T}=\mathcal{U}\mathcal{K}$, where $\mathcal{K}$ is the complex conjugate operator associated with the TR operation respected by Maxwell systems in general. Since $\mathcal{T}^2=-1$ is guaranteed by $\mathcal{U}^2=-1$, $\mathcal{T}$ can be taken as a pseudo-TR operator that provides Kramers doubling in the same way as TR symmetry in electronic systems. It is clear that the crystal symmetry plays an important role in this pseudo-TR symmetry [36].

The two pseudospin states are given by

$$p_\pm=(p_x\pm ip_y)/\sqrt{2};\quad d_\pm=(d_{x^2-y^2}\pm id_{xy})/\sqrt{2}, \tag{4}$$

which are related to the above basis functions by unitary transformation (see Supplemental Material [37]). Namely, the up and down pseudospins correspond to positive and negative angular momenta of the wave function of the $E_z$ field. The in-plane magnetic fields associated with $p_\pm$ and $d_\pm$ in Eq. (4) are shown in Fig. 2(b). The physics discussed above applies also for $K$ and $K'$ points with 2D irreducible representations.

Pseudospins discussed so far in photonic systems include bonding (antibonding) states of electric and magnetic fields [24,25], left-hand (right-hand) circular polarizations of EM waves [28], and clockwise (anticlockwise) circulations of light in CROWs [29,30].

*Photonic bands.*—Now we calculate the photonic band dispersions described by the master equation (1) imposing periodic boundary conditions along unit vectors $\vec{a}_1$ and $\vec{a}_2$ given in Fig. 1. As shown in Fig. 3, double degeneracy in the band dispersions appears at the Γ point, which can be identified as $p_\pm$ and $d_\pm$ states, consistent with the symmetry consideration. For large lattice constant $a_0$, the photonic band below (above) the gap is occupied by $p_\pm$ ($d_\pm$) states [see Fig. 3(a) for $a_0/R = 3.125$ with $R$ the length of hexagon edge].

Reducing the lattice constant to $a_0/R = 3$, the $p$ and $d$ states become degenerate at the Γ point, and two Dirac cones appear as shown in Fig. 3(b). This is because at this lattice constant the system is equivalent to the honeycomb lattice of individual cylinders, and the doubly degenerate Dirac cones are nothing but those at the $K$ and $K'$ point in the Brillouin zone of honeycomb lattice based on the primitive rhombic unit cell of two sites [31].

When the lattice constant is further reduced, a global photonic band gap is reopened near the Dirac point as shown in Fig. 3(c) for $a_0/R = 2.9$. Now the $E_z$ field at the low- (high-) frequency side of the band gap exhibits $d_\pm$ ($p_\pm$) characters around the Γ point, opposite to the order away from the Γ point. Namely, a band inversion takes place upon reducing the lattice constant in the present system. Quantitatively, the band gap is $\Delta\omega = 5.47$ THz at $\omega = 138.77$ THz with $a_0 = 1$ μm, with all the quantities scaling with the lattice constant.

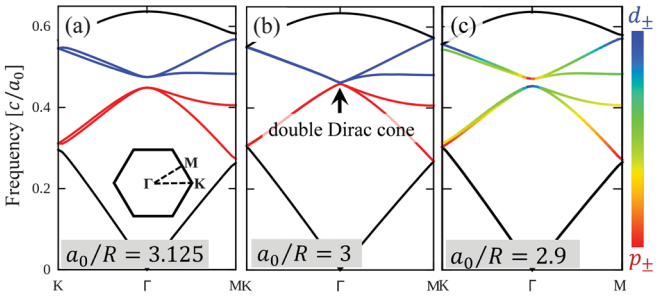


FIG. 3 (color). Dispersion relations of the TM mode for the 2D photonic crystals with $\varepsilon_d = 11.7$, $\varepsilon_A = 1$, and $d = 2R/3$ for (a) $a_0/R = 3.125$ (Inset: Brillouin zone of triangular lattice), (b) $a_0/R = 3$, and (c) $a_0/R = 2.9$. Blue and red are for $d_\pm$ and $p_\pm$ bands, respectively, and rainbow for hybridization between them. The case of $a_0/R = 3$ corresponds exactly to the honeycomb lattice of individual cylinders.

In order to see what happens in the system around the band inversion, we check the real-space distribution of the pseudospin specific Poynting vector $\vec{S} = \mathrm{Re}[\vec{E} \times \vec{H}^*]/2$ averaged over a period $\tau = 2\pi/\omega$, which describes the energy flow in the present EM system. It is found that the Poynting vector is circling around individual atoms as shown in Fig. 4(a) for $a_0/R = 3.125$, with the chirality of the Poynting vector corresponding to the pseudospin (Poynting vector for pseudospin-up is not shown explicitly). The EM energy flows around individual atoms, characterizing a conventional "insulating" state. At $a_0/R = 2.9$, namely, after the band inversion, the Poynting vectors are much enhanced in interstitial regimes as shown in Fig. 4(b). It is in a sharp contrast to the case in Fig. 4(a), and hints at an unconventional insulating state.

Although Dirac dispersions in photonic systems were discussed previously in both square and triangular lattices [42–44], possible nontrivial topology was not addressed.

*Topological edge state.*—We also consider a ribbon of photonic crystal after band inversion by cladding its two edges in terms of two photonic crystals with trivial band gap (namely, before band inversion) at the same frequency window, which prevents possible edge states from leaking into free space. It should be kept in mind that, since the cluster of six cylinders is the basic block of the present design, we keep it intact for discussions of the main physics. As displayed in Fig. 5(a), there appear additional states as indicated by the double degenerate red curves within the bulk gap. Checking the real-space distribution of the $E_z$ field at typical momenta around the Γ point [$A$ and $B$ in the enlarged vision of Fig. 5(a) with $k_x = \pm 0.04(2\pi/a_0)$], we find that the in-gap states locate at the ribbon edges and decay exponentially into bulk as displayed in Fig. 5(b) (two other states are localized at the other ribbon edge and are not shown explicitly). As shown in the right insets of Fig. 5(b), the Poynting vectors exhibit a nonzero downward (upward) EM energy flow for the pseudospin-up (pseudospin-down) state even averaged

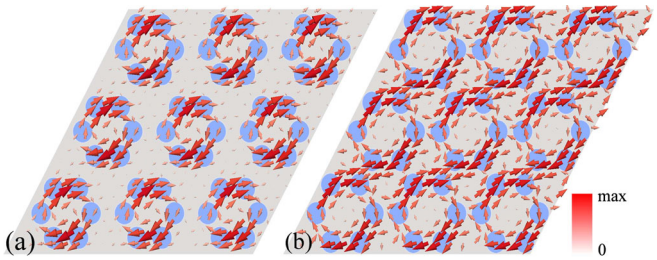


FIG. 4 (color online). Real-space distributions of the time-averaged Poynting vector associated with the pseudospin-down state at the Γ point below the photonic gap: (a) $a_0/R = 3.125$ in the trivial regime and (b) $a_0/R = 2.9$ in the topological regime. Other parameters are taken same as those in Fig. 3.

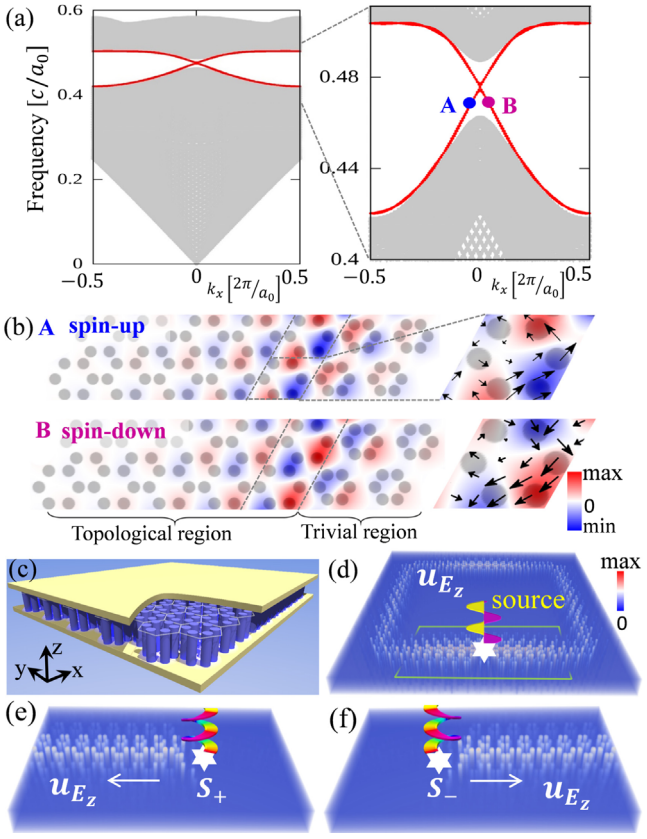


FIG. 5 (color online). (a) Dispersion relation of a ribbon-shaped 2D topological photonic crystal, which is infinite in one direction and of 45 and 6 artificial atoms for the topological and trivial regions respectively in the other direction. Right panel: enlarged view of (a) around the band gap. Dark gray (Red) curves are for topological edge states. (b) Real-space distributions of $E_z$ fields at points A and B indicated in the right panel of (a). Right panels: time-averaged Poynting vectors $\vec{S}$ over a period. (c) 3D photonic crystal of height $h$ with two horizontal gold plates placed at two ends symmetrically. (d) Distribution of energy-density of $E_z$ field $u_{E_z}(\mathbf{r}) = \varepsilon(\mathbf{r})|E_z(\mathbf{r})|^2/2$ in the 3D topological photonic crystal in (c) stimulated by a linearly polarized source. (e) Leftward and (f) rightward unidirectional energy propagation stimulated by source $S_+$ and $S_-$, which injects $E_z$ field with wave function of positive and negative, respectively, angular momentum in the region denoted by gray (green) solid frame in (d). The lattice constant and diameter of cylinder are kept same in the whole space $a_0 = 1$ $\mu$m and $d = 0.24$ $\mu$m, while the edge length of hexagon is $R = 0.345a_0$ $(a_0/R = 2.9)$ and $R = 0.32a_0$ $(a_0/R = 3.125)$ in topological and trivial regions, and the frequency of all sources is $\omega = 135.6$ THz within the topological band gap. In the 3D system the height of cylinder is $h = 1$ $\mu$m. Other parameters are same as those in Fig. 3.

over time. This indicates unambiguously counterpropagations of EM energy at the sample edge associated with the two pseudospin states, the hallmark of a quantum spin Hall effect (QSHE) state [2,3]. Distributions of the Poynting vectors of the bulk bands in Fig. 5(b) for the ribbon system are similar to those in Fig. 4(b) for the infinite system. QHE has been described by the cyclic motions of electrons under strong external magnetic field in a quasiclassic picture of electronic wave functions [45]. Note that the Poynting vector describes energy flows in systems governed by Maxwell equations, and therefore the distributions shown in Figs. 4 and 5(b) can be observed in experiments. The photonic QSHE in the present system can also be confirmed by evaluating the $\mathbb{Z}_2$ topology index based on a $k \cdot p$ model around the $\Gamma$ point (see Supplemental Material [37]).

Since the pseudo-TR symmetry and the pseudospin rely on the $C_6$ symmetry, deformations in the system that break the crystalline order and thus the pseudo-TR symmetry would mix the two pseudospin channels as in other $\mathbb{Z}_2$ topological photonic systems [24,29]. Actually, there is a tiny gap at the $\Gamma$ point in Fig. 5(a) (unnoticeable in the present scale) due to the reduction of $C_6$ crystalline symmetry at the ribbon edge. However, the photonic topology remains valid up to moderate deformations as far as the dispersions of edge states are not pushed into bulk bands (see Supplemental Material [37]).

For experimental implementation of the present topological state, the finite height of cylinders along the $z$ direction has to be taken into account. We consider a square sample of topological photonic crystal sandwiched by two horizontal gold plates [see Fig. 5(c)] with separation $h$ chosen to prevent photonic bands with nonzero $k_z$ from falling into the topological band gap. Damping of EM waves in gold plates is taken into account by adopting a complex reflective index for gold. The size of the topological sample is $40\vec{a}_1 \times 20(\vec{a}_1 + \vec{a}_2)$ with all four edges clad by a trivial photonic crystal. A harmonic line source $\mathbf{E} = E_0 e^{i\omega t}\hat{z}$ is placed parallel to dielectric cylinders to inject the EM wave at the interface with the frequency in the topological band gap. We simulate the 3D system by solving time-dependent Maxwell equations using the finite difference time-domain method [46] implemented in the MIT electromagnetic equation propagation (MEEP) [47]. Since any harmonic source preserves TR symmetry respected by the Maxwell equations, the system exhibits helical topological edge states as shown in Fig. 5(d). When an EM wave characterized by an $E_z$ field with wave function of positive (negative) angular momentum is injected by line source $S_+$ $(S_-)$ [48], leftward (rightward) unidirectional energy propagation takes place [see Figs. 5(e) and (f)], as expected from the bulk topology.

In conclusion, we derive a two-dimensional photonic crystal with nontrivial topology purely based on conventional dielectric material, simply by deforming a honeycomb lattice of cylinders. A pseudo-time-reversal symmetry is constructed in terms of the time reversal symmetry respected by the Maxwell equations in general and the $C_6$ crystal symmetry upon design, which enables the Kramers doubling with the role of pseudospin played by the angular momentum of wave functions of the out-of-plane electric field of transverse magnetic modes. The

present topological photonic crystal with simple design backed up by the symmetry consideration can be fabricated relatively easily as compared with other proposals, and is expected to leave impacts on topological physics and related materials sciences.

The authors acknowledge K. Sakoda and T. Ochiai for useful discussions. This work was supported by the WPI Initiative on Materials Nanoarchitectonics, Ministry of Education, Culture, Sports, Science and Technology of Japan, and partially by Grant-in-Aid for Scientific Research under the Innovative Area "Topological Quantum Phenomena" (No. 25103723), Ministry of Education, Culture, Sports, Science and Technology of Japan.

*To whom all correspondence should be addressed. HU.Xiao@nims.go.jp

[1] K. v. Klitzing, G. Dorda, and M. Pepper, Phys. Rev. Lett. **45**, 494 (1980).
[2] M. Z. Hasan and C. L. Kane, Rev. Mod. Phys. **82**, 3045 (2010).
[3] X.-L. Qi and S.-C. Zhang, Rev. Mod. Phys. **83**, 1057 (2011).
[4] D. J. Thouless, M. Kohmoto, M. P. Nightingale, and M. den Nijs, Phys. Rev. Lett. **49**, 405 (1982).
[5] D. Xiao, M.-C. Chang, and Q. Niu, Rev. Mod. Phys. **82**, 1959 (2010).
[6] F. D. M. Haldane, Phys. Rev. Lett. **61**, 2015 (1988).
[7] C. L. Kane and E. J. Mele, Phys. Rev. Lett. **95**, 226801 (2005).
[8] B. A. Bernevig, T. L. Hughes, and S.-C. Zhang, Science **314**, 1757 (2006).
[9] D. Hsieh, D. Qian, L. Wray, Y. Xia, Y. S. Hor, R. J. Cava, and M. Z. Hasan, Nature (London) **452**, 970 (2008).
[10] R. Yu, W. Zhang, H.-J. Zhang, S.-C. Zhang, X. Dai, and Z. Fang, Science **329**, 61 (2010).
[11] C.-Z. Chang *et al.*, Science **340**, 167 (2013).
[12] D. Pesin and A. H. MacDonald, Nat. Mater. **11**, 409 (2012).
[13] Q.-F. Liang, L.-H. Wu, and X. Hu, New J. Phys. **15**, 063031 (2013).
[14] C. Nayak, S. H. Simon, A. Stern, M. Freedman, and S. Das Sarma, Rev. Mod. Phys. **80**, 1083 (2008).
[15] T. D. Stanescu and S. Tewari, J. Phys. Condens. Matter **25**, 233201 (2013).
[16] C. W. J. Beenakker, Annu. Rev. Condens. Matter Phys. **4**, 113 (2013).
[17] L.-H. Wu, Q.-F. Liang, and X. Hu, Sci. Tech. Adv. Mater. **15**, 064402 (2014).
[18] E. Yablonovitch, Phys. Rev. Lett. **58**, 2059 (1987).
[19] J. B. Pendry, A. J. Holden, D. J. Robbins, and W. J. Stewart, IEEE Trans. Microwave Theory Tech. **47**, 2075 (1999).
[20] F. D. M. Haldane and S. Raghu, Phys. Rev. Lett. **100**, 013904 (2008).
[21] Z. Wang, Y. D. Chong, J. D. Joannopoulos, and M. Soljačić, Phys. Rev. Lett. **100**, 013905 (2008).
[22] Z. Wang, Y. Chong, J. D. Joannopoulos, and M. Soljačić, Nature (London) **461**, 772 (2009).
[23] K. Fang, Z. Yu, and S. Fan, Nat. Photonics **6**, 782 (2012).
[24] A. B. Khanikaev, S. H. Mousavi, W.-K. Tse, M. Kargarian, A. H. MacDonald, and G. Shvets, Nat. Mater. **12**, 233 (2013).
[25] T. Ma, A. B. Khanikaev, S. H. Mousavi, and G. Shvets, arXiv:1401.1276.
[26] G. Q. Liang and Y. D. Chong, Phys. Rev. Lett. **110**, 203904 (2013).
[27] M. C. Rechtsman, J. M. Zeuner, Y. Plotnik, Y. Lumer, D. Podolsky, F. Dreisow, S. Nolte, M. Segev, and A. Szameit, Nature (London) **496**, 196 (2013).
[28] C. He, X.-C. Sun, X.-P. Liu, M.-H. Lu, Y. Chen, L. Feng, and Y.-F. Chen, arXiv:1405.2869.
[29] M. Hafezi, E. A. Demler, M. D. Lukin, and J. M. Taylor, Nat. Phys. **7**, 907 (2011).
[30] M. Hafezi, S. Mittal, J. Fan, A. Migdall, and J. M. Taylor, Nat. Photonics **7**, 1001 (2013).
[31] T. Ochiai, Phys. Rev. B **86**, 075152 (2012); Int. J. Mod. Phys. B **28**, 1441004 (2014).
[32] L. Lu, J. D. Joannopoulos, and M. Soljačić, Nat. Photonics **8**, 821 (2014).
[33] J. D. Joannopoulos, S. G. Johnson, J. N. Winn, and R. D. Meade, *Photonic Crystals: Molding the Flow of Light* (Princeton University Press, New Jersey, 2008).
[34] S. G. Johnson and J. D. Joannopoulos, Opt. Express **8**, 173 (2001).
[35] M. S. Dresselhaus, G. Dresselhaus, and A. Jorio, *Group Theory: Application to the Physics of Condensed Matter* (Springer-Verlag, Berlin, Heidelberg, 2008).
[36] L. Fu, Phys. Rev. Lett. **106**, 106802 (2011).
[37] See Supplemental Material at http://link.aps.org/supplemental/10.1103/PhysRevLett.114.223901 for discussions of pseudo-time-reversal symmetry, effective $k \cdot p$ Hamiltonian and propagations of edge states, which includes Refs. [38–41].
[38] E. Prodan, Phys. Rev. B **80**, 125327 (2009).
[39] Y. Yang, Z. Xu, L. Sheng, B. Wang, D. Y. Xing, and D. N. Sheng, Phys. Rev. Lett. **107**, 066602 (2011).
[40] S. Hughes, L. Ramunno, J. F. Young, and J. E. Sipe, Phys. Rev. Lett. **94**, 033903 (2005).
[41] S. Mazoyer, J. P. Hugonin, and P. Lalanne, Phys. Rev. Lett. **103**, 063903 (2009).
[42] X. Huang, Y. Lai, Z. H. Hang, H. Zheng, and C. T. Chan, Nat. Mater. **10**, 582 (2011).
[43] K. Sakoda, Opt. Express **20**, 9925 (2012).
[44] K. Sakoda, Opt. Express **20**, 3898 (2012).
[45] S. M. Girvin, *The Quantum Hall Effect: Novel Excitations and Broken Symmetries* (Springer-Verlag, Berlin, Heidelberg, 1999).
[46] A. Taflove and S. C. Hagness, *Computational Electrodynamics: The Finite-Difference Time-Domain Method* (Artech: Norwood, MA, 2000).
[47] A. F. Oskooi, D. Roundy, M. Ibanescu, P. Bermel, J. D. Joannopoulos, and S. G. Johnson, Comput. Phys. Commun. **181**, 687 (2010).
[48] In real experiments, one prepares source $S_+(S_-)$ in terms $H_0 e^{i\omega t}(\hat{x} \mp i\hat{y})$ with $H_0$ an arbitrary amplitude, $\omega$ a frequency and $\hat{x}(\hat{y})$ the unit vector along $x(y)$ direction, which generates in-plane magnetic field with anticlockwisely (clockwisely) circular polarization, and thus the out-of-plane $E_z$ field with wave function of positive (negative) angular momentum (see Supplemental Material [37]).